Nano Research
2024, 17(6): 4687–4692
ISSN 1998-0124 CN 11-5974/O4
https://doi.org/10.1007/s12274-023-5473-9

Research Article

Core–shell nanoparticle enhanced Raman spectroscopy *in situ* probing the composition and evolution of interfacial species on PtCo surfaces

Jing Liu[1], Han-Liang Zhong[2], Xiangyu Li[1], Mu-Fei Yue[3], Wei-Min Yang[3], Xueqiu You[1] (✉), Jing-Hua Tian[4] (✉), Yao-Hui Wang[3] (✉), and Jian-Feng Li[3,4,5] (✉)

[1] *Fujian Provincial Key Laboratory of Oceanic Information Perception and Intelligent Processing, School of Ocean Information Engineering, Jimei University, Xiamen 361021, China*
[2] *College of Chemistry, Fuzhou University, Fuzhou 350108, China*
[3] *State Key Laboratory of Physical Chemistry of Solid Surfaces, MOE Key Laboratory of Spectrochemical Analysis and Instrumentation, iChEM, College of Chemistry and Chemical Engineering, College of Materials, College of Energy, Xiamen University, Xiamen 361005, China*
[4] *Innovation Laboratory for Sciences and Technologies of Energy Materials of Fujian Province (IKKEM), Xiamen 361005, China*
[5] *Shenzhen Research Institute of Xiamen University, Shenzhen 518000, China*

Received: 17 November 2022 / **Revised:** 26 December 2022 / **Accepted:** 2 January 2023

ABSTRACT

The composition and evolution of interfacial species play a key role during electrocatalytic process. Unveiling the structural evolution and intermediate during catalytic process by *in situ* characterization can shed new light on the electrocatalytic reaction mechanism and develop highly efficient catalyst. However, directly probing the interfacial species is extremely difficult for most spectroscopic techniques due to complicated interfacial environment and ultra-low surface concentration. Herein, electrochemical core–shell nanoparticle enhanced Raman spectroscopy is utilized to probe the composition and evolution processes of interfacial species on Au@Pt, Au@Co, and Au@PtCo core–shell nanoparticle surfaces. The spectral evidences of interfacial intermediates including hydroxide radical (OH*), superoxide ion (O_2^-), as well as metal oxide species are directly captured by *in situ* Raman spectroscopy, which are further confirmed by the both isotopic experiment and density functional theory calculation. These results provide a mechanistic guideline for the rational design of highly efficient electrocatalysts.

KEYWORDS

in situ Raman, core–shell nanoparticle, PtCo, interfacial species, composition and evolution

1 Introduction

Recently, an important issue in heterogeneous catalysis is how to unveil and understand the electrochemical interface at the molecular or even atomic level [1, 2]. Direct monitoring of the composition and evolution of interfacial species has always been an important field in the electrochemical process, and will greatly contribute to designing and developing more efficient catalysts [3–5]. Transition metal catalysts represented by platinum, which are extensively used and involved in many classical electrocatalytic reactions, such as oxygen reduction reaction (ORR), hydrogen evolution reaction (HER), and hydrogen oxidation reaction (HOR), have been the focus of energy conversion for a long time [6, 7]. The composition and evolution of species at electrocatalyst interface play a key role in determining the activity of catalyst, and thus *in situ* characterization is of great significance [8, 9]. Although many research teams have revealed the roles of the structure and composition of the catalyst itself by experimental and theoretical methods, the detailed composition and evolution of interface species are still not clear.

Optimizing the composition and structure of catalyst to tune the catalytic performance is widely used in the design of efficient catalyst [10–13]. Besides, tuning the interfacial species can also lead a significantly improved performance [6, 14, 15]. Markovic et al. realized an improved activity in the hydrogen/oxygen evolution as well as CO oxidation by introducing an oxophilic metal on Pt catalyst surface to increase the adsorption of hydroxide radical (OH*), proposing consecutively that the strength of the OH-M as a descriptor for catalytic activity [1, 15, 16]. Zhuang et al. studied the influence of hydroxide anion (OH^-) during the hydrogen oxidation reaction by using surface-controlled PtNi alloy nanoparticles (NPs) as the model catalysts [17]. Our group revealed the key role of interfacial water toward the HER on Pd single crystal surfaces, revealing that structurally ordered interfacial water molecules lead to a high-efficiency HER rate [2]. Due to these remarkable regulation strategies, the catalytic activity has been greatly improved. However, the interfacial species on Pt-based catalyst is still not clear even until today, thus, resulting in a slow progress about catalytic mechanism understanding.

Raman spectroscopy with fingerprint identification is a powerful tool to study catalyst itself and intermediate species

Address correspondence to Xueqiu You, youxueqiuqqq@126.com; Jing-Hua Tian, jhtian@xmu.edu.cn; Yao-Hui Wang, yaohuiwang@xmu.edu.cn; Jian-Feng Li, li@xmu.edu.cn

adsorbed on catalyst surface [18, 19]. However, normal Raman spectroscopy is hard to monitor intermediates due to its low sensitivity towards interfacial species. Surface-enhanced Raman spectroscopy (SERS) was invented to overcome the flaw of Raman spectroscopy. SERS greatly improves the sensitivity of Raman spectroscopy by using Au, Ag, and Cu, etc. nanostructures as enhanced substrates, as low as a single molecule level [20, 21], and has been widely applied in various fields. Nevertheless, only Au, Ag, and Cu nanostructured materials as SERS substrates possess high Raman enhancement, while catalytically active transition metals exhibit very low Raman enhancement, which limits the application of SERS in catalysis studies [22].

In this work, an extensive SERS method, named core–shell nanoparticle enhanced Raman spectroscopy (CSERS), is used to probe the composition and evolution processes of interfacial species on transition metal surfaces (representative pure Pt, pure Co, and PtCo alloy here). We construct core–shell nanostructures being consist of Au as a core and catalyst materials (Pt, Co, and PtCo alloy) as shells, in which the Au core is the Raman amplifier to enhance the signals from catalyst shell surface. Combing the both direct spectral evidence of interfacial species and density functional theory (DFT) calculations, the composition and evolution processes of interfacial species on catalyst surfaces are *in situ* elucidated at the molecular and atomic level.

2 Results and discussions

The structural information about commercial 40 wt.% Pt/C catalyst was analyzed by the normal Raman spectroscopy, two strong D and G bands being assigned to carbon as well as a weak and broad band at the range of 300–700 cm^{-1} ascribed to PtO_x are presented in Fig. 1(a) [23, 24]. These results verify that the interfacial structure is difficult to be resolved by normal Raman spectroscopy because of its weak Raman enhancements of Pt NPs. Besides, the three-dimensional-finite-difference time-domain (3D-FDTD) results show that the maximum Raman enhancement of pure Pt NPs (5 nm in diameter) is only 10^3 times (Fig. S1(a) in the Electronic Supplementary Materail (ESM)).

Schematic diagram (Fig. 1(b)) shows the enhanced mode of core–shell NPs (transmission electron microscopy (TEM) image of core–shell NPs in Fig. 1(c)). The Au NPs around 55 nm in diameter are used as the core and Pt-based materials around 1.4 nm thickness are coated on the Au NPs to form core–shell nanostructures. The maximum enhancement of core–shell nanostructure is 10^8 times, much larger than that of pure Pt NPs (Fig. S1(b) in the ESM), indicating that CSERS can directly detect interfacial species on Pt-based materials surface.

X-ray diffraction (XRD) was carried out to examine lattice parameters of Au@Pt and Au@PtCo core–shell NPs (Fig. 1(d)). The XRD results of Au@PtCo and Au@Pt catalysts show analogous diffraction peak positions to Au and Pt, respectively. The higher diffraction angle of the Au@PtCo XRD curve indicates the formation of a PtCo alloy. As evidenced by inductively coupled plasma optical emission spectrometry (ICP-OES) measurements, the content of PtCo shell in Au@PtCo colloidal solutions is shown in Table S1 in the ESM with the atomic ratio of Pt:Co being around 6.7:1.

The Raman spectra of Au@Pt, Au@Co, and Au@PtCo in air were obtained by CSERS, as shown in Fig. 2(a). Four bands are observed in the spectrum of Au@Co. According to the normal Raman spectra of α-$Co(OH)_2$ and CoOOH in Refs. [25, 26], the broad band at the wavenumber from 400 to 700 cm^{-1} is attributed to the collection of bivalent Co (Co^{2+}) and trivalent Co (Co^{3+}) from α-$Co(OH)_2$ and CoO_x matters. The surface valence of Co shell (Au@Co NPs) was further investigated by X-ray photoelectron spectroscopy (XPS). As shown in Fig. S2 in the ESM, four pairs of peaks can be obtained after fitting the original data. The peaks at 776.9 and 793.7 eV corresponding to Co $2p_{3/2}$ and Co $2p_{1/2}$ respectively represent unoxidized metallic Co (Co^0). The peaks at 781.6 (Co $2p_{3/2}$) and 797.4 eV (Co $2p_{1/2}$) represent Co^{2+}. The peaks at 785.1 (Co $2p_{3/2}$) and 803.1 eV (Co $2p_{1/2}$) represent Co^{3+}. Besides, a pair of satellite peaks locate at 788.2 (Co $2p_{3/2}$) and 806.9 eV (Co $2p_{1/2}$). These Raman and XPS results indicate that the shell contains pure Co, α-$Co(OH)_2$, and CoOOH. A broad band at the range of 400–700 cm^{-1} is well observed in Au@Pt CSERS spectrum, which is attributed to PtO_x species [24]. The CSERS spectrum of Au@PtCo shows two obvious bands about CoO_x and PtO_x species. These results clearly confirm that there are abundant oxygen containing species on catalyst surfaces.

Electrochemical cyclic voltammograms (CVs) were used to study the behaviors of Au@Pt, Au@Co, and Au@PtCo NPs under alkaline condition (Ar-saturated 0.1 M KOH solution). The CV of pure Au NPs is shown in Fig. S3 in the ESM as a reference. The whole potential windows in the CVs are discussed by dividing into

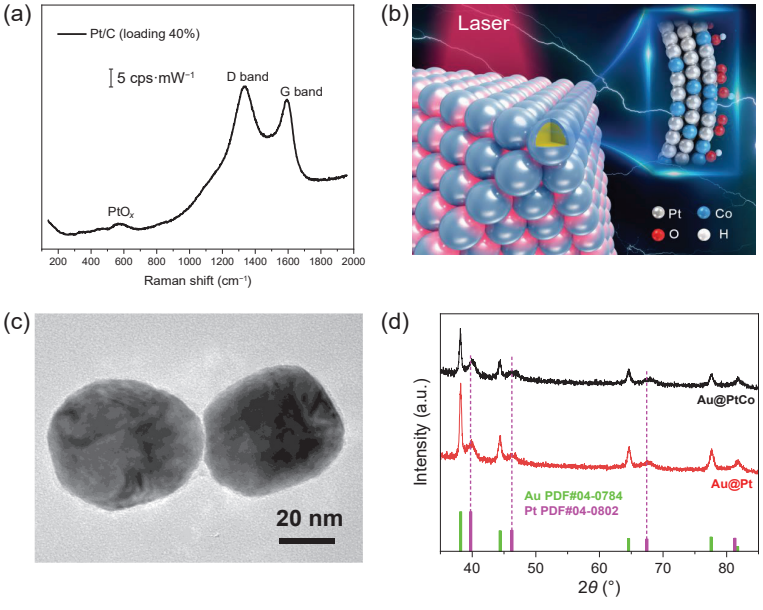

Figure 1 Characteristics of core–shell nanoparticles. (a) Normal Raman spectrum of Pt/C catalyst (Pt 40% loading). (b) Schematic diagram about the enhanced mode of core–shell NPs. (c) TEM image of Au@PtCo NPs. (d) XRD patterns of Au@Pt and Au@PtCo and the standard patterns of Au and Pt.

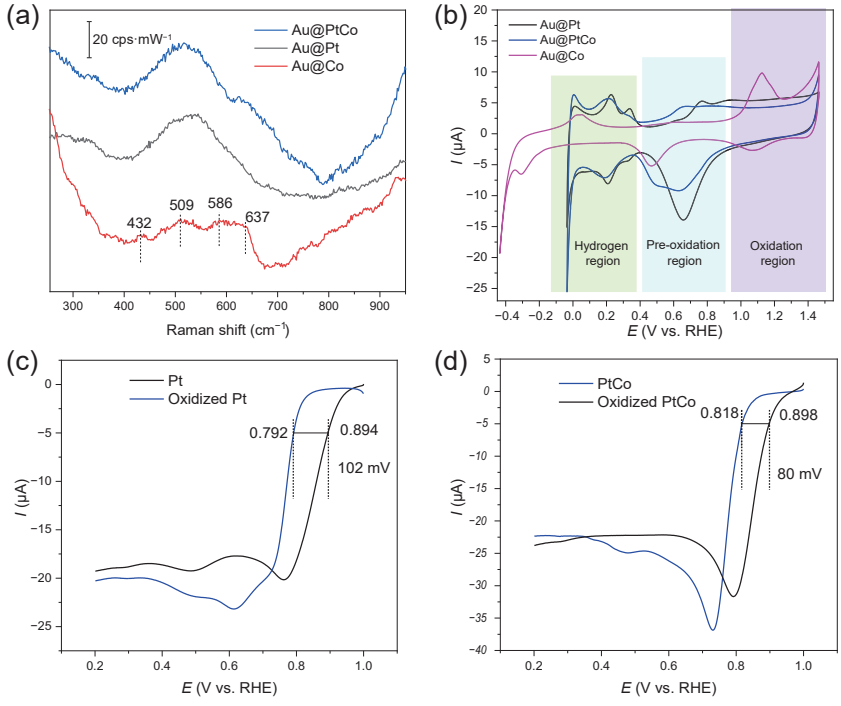

Figure 2 Spectral and electrochemical behaviors of core–shell NPs. (a) CSERS spectra of Au@Co NPs, Au@Pt NPs, and Au@PtCo NPs under air condition. (b) CVs of Au@Co, Au@Pt, and Au@PtCo NPs in Ar-saturated 0.1 M KOH with a scan rate of 50 mV·s^{-1}. ORR activity of (c) Au@Pt and (d) Au@PtCo NPs with oxide and without oxide in O_2-saturated 0.1 M KOH solution with a scan rate of 10 mV·s^{-1}.

hydrogen region, pre-oxidation region, as well as oxidation region. In hydrogen region (Fig. 2(b)), there are no obvious hydrogen adsorption/desorption peaks on Co surface in the CV of Au@Co NPs. A pair of redox peaks at −0.3 and 0.04 V versus the reversible hydrogen electrode (RHE) are observed, attributing to the α-$Co(OH)_2$ to metallic Co in accordance with the previous results [27]. We only observed the hydrogen adsorption/desorption on Pt surface at the range of 0–0.4 V in the CVs of Au@Pt and Au@PtCo NPs.

Meanwhile, in pre-oxidation region, the oxidation/reduction peaks between 0.4–0.7 V are observed in the CV of Au@Co NPs due to the phase transformation of a random α-$Co(OH)_2$ phase to an ordered α-$Co(OH)_2$ phase, according to the previous scanning tunneling microscopy (STM) results and our *in situ* Raman results (detailed Raman discussion later). A broad pre-oxidation peak at around 0.77 V and a reduction peak at 0.66 V are observed in the CV of Au@Pt NPs. The oxidation/reduction peaks about Co and Pt appear synchronously in the CV of Au@PtCo, indicating that the Co and Pt exist in the shell.

In oxidation region, obvious oxidation/reduction peaks at 1.12/1.07 V about the Co^{2+} to Co^{3+} transition are observed in the CV of Au@Co in linear with the previous results [25]. However, there are no obvious Co^{2+} to Co^{3+} transition peaks in the CVs of Au@Pt and Au@PtCo. The PtCo alloy formation causes a hysteresis about the transition of Co^{2+} to Co^{3+} during electrochemical process.

We further studied the role of oxygen species on Au@Pt, Au@Co, and Au@PtCo NPs surfaces during ORR process, as shown in Figs. 2(c) and 2(d). A 102 mV overpotential attenuation at 5 μA current is observed according to the ORR linear sweep voltammetry curves of Au@Pt (0.894 V) and oxidized Au@Pt (0.792 V) surfaces due to the adsorption of oxygen species. However, only 80 mV attenuation is observed on Au@PtCo (0.898 V) and oxidized Au@PtCo (0.818 V) surfaces. The PtCo alloy is more stable than pure Pt, resulting in the exposure of more active sites toward ORR [28].

The evolution processes of oxygen species on Au@Co surface in a 0.1 M KOH solution are probed by the *in situ* CSERS. Three obvious Raman bands at 426, 502, and 860 cm^{-1} at 0.165 V initial potential are observed in the spectra (Fig. 3(a)). The frequencies and shapes of bands at 426 and 502 cm^{-1} are similar to those of α-$Co(OH)_2$ according to the normal Raman results [25]. The electrochemical CV results also show the formation of α-$Co(OH)_2$ at 0.165 V. Therefore, these two bands are attributed to the Co–O vibrations of α-$Co(OH)_2$. To further confirm the attribution of Raman bands, a D_2O isotopic substitution experiment was carried out under same experimental condition. We find that the bands at 426 and 502 cm^{-1} shift to 415 and 482 cm^{-1}, respectively, in the D_2O isotopic experiment (Fig. 3(b)). Considering the difficult replacement of bulk OH in $Co(OH)_2$ and only 11 or 17 cm^{-1} wavenumber shifts indicate that the formation of hydrogen bonds between the α-$Co(OH)_2$ and H_2O (α-$Co(OH)_2$···H_2O). The hydrogen bond networks cause such a small wavenumber shift. In addition, the band at 860 shifts to 645 cm^{-1} (75% wavenumber shift) in D_2O experiment, indicating that the band is assigned to OH* species. DFT calculation was used to confirm the detailed attribution and adsorbed sites about OH*. The DFT results show that the frequency of Co–O–H bending mode of OH* on Co top site of α-$Co(OH)_2$ (111) locates at 862 cm^{-1}, being closest to the experimental results (Figs. 3(c) and 3(d) and Table S2 in the ESM). Meanwhile, the *in situ* CSERS spectra and CV of Au@Co both demonstrate that α-$Co(OH)_2$ exists in shell at the presence of OH* potential range (0.165–0.765 V). Therefore, this band at 860 cm^{-1} is attributed to OH* adsorbed on a Co top site of α-$Co(OH)_2$. This band fades away at 0.765 V due to the deprotonation process of α-$Co(OH)_2$ to CoO_x species.

The intensity of band at 426 cm^{-1} increases with the potential shifting from 0.165 to 0.665 V, then decreases until 0.965 V. The intensity of band located at 502 cm^{-1} decreases with the potential shifting from 0.165 to 0.465 V, then increases until 0.665 V. Both bands fade away at 1.065 V. Meanwhile, the band width at half height of 502 cm^{-1} becomes narrow after 0.465 V, indicating the formation of more ordered phase of α-$Co(OH)_2$, which is consist with the phase transformation peak from 0.4 to 0.7 V in the CV of Au@Co. A new band at around 568 cm^{-1} appears at 0.765 V,

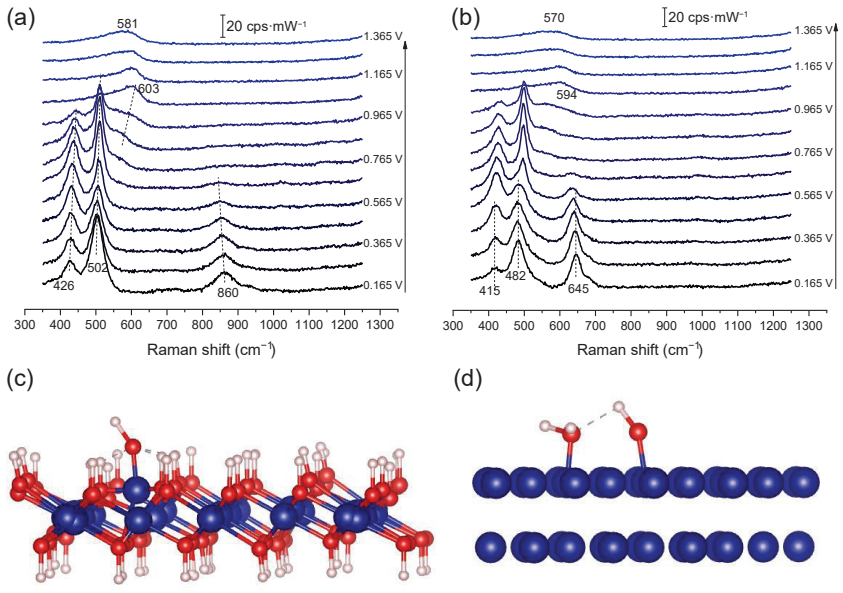

Figure 3 Raman and DFT results. Electrochemical *in situ* CSERS spectra of Au@Co in 0.1 M KOH ((a) H_2O and (b) D_2O) solution. DFT calculated models of OH* adsorbed on (c) $Co(OH)_2$ (111) and (d) Co (111) surfaces with a Co top site. Ru, O, and H atoms are showed as blue, red, and white balls, respectively.

which is attributed to CoO_x with +3 valence. This band shifts to 558 cm^{-1} in D_2O experiment indicating the formation of hydrogen bonds between the CoO_x and H_2O. This band becomes stronger and shifts to 603 cm^{-1} at 1.065 V, finally being stable at 1.365 V.

We investigated the evolution processes of interfacial species on Au@Pt surface in alkaline condition (Fig. 4(a)), which are like the Au@Co *in situ* CSERS experiment. As the potential positively shifts from 0.165 V, a band centered at 1142 cm^{-1} appears at 0.365 V. With a further increase in the potential, this band becomes stronger until 0.665 V, and then disappears at 0.965 V. A D_2O isotopic substitution experiment was also conducted to confirm the attribution of Raman band, and we find that the band at 1142 cm^{-1} does not exhibit obvious shifts (Fig. S4 in the ESM). Thus, this species at 1142 cm^{-1} is supposed to contain no H atoms. DFT results show that a close frequency of O–O stretching mode of O_2^- on Pt (111) with top site is 1177 cm^{-1} (calculated model in Fig. 4(c)). Meanwhile, the previous results [29] also point that the frequency of O_2^- on Pt (111) surface in alkaline condition locates at 1150 cm^{-1}, closing to our results. Therefore, according to above information, we confirm that the band at 1142 cm^{-1} should be attributed to the O–O stretching mode of O_2^- on Pt (111) with a top site. A broad Raman band centered at 569 cm^{-1} appears at 0.965 V and the intensity of this band becomes strong when the potential continues to increase to 1.365 V. This band is attributed to Pt–O vibration of PtO_x species.

We further investigated the evolution processes of interfacial species on Au@PtCo surface in an alkaline solution. Two Raman bands at 853 and 1152 cm^{-1} are observed (Fig. 4(b)). Same D_2O experiment was carried to confirm the band attribution as shown in Fig. S5 in the ESM. The Raman band at 853 shifts to 674 cm^{-1}

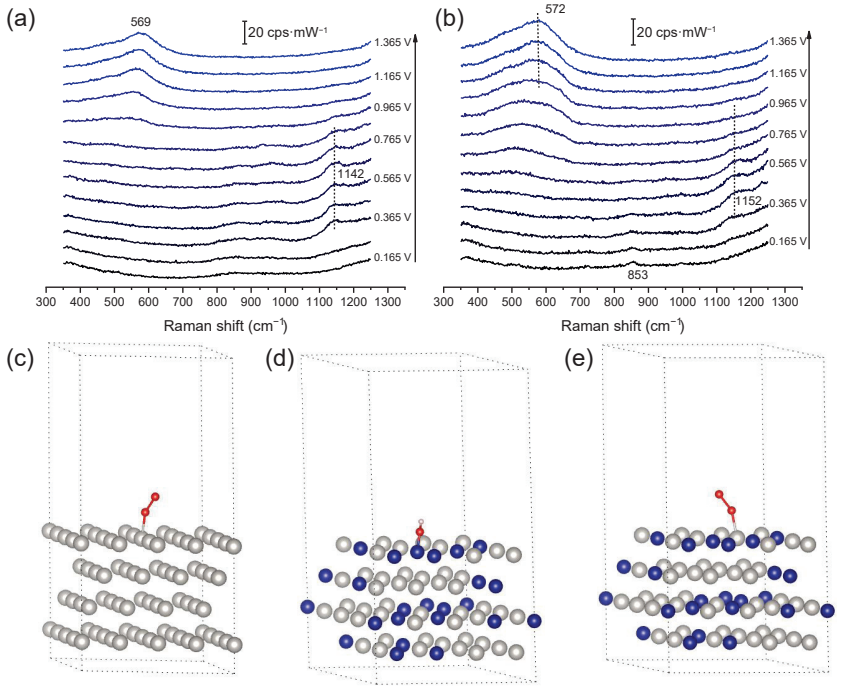

Figure 4 Raman and DFT results. Electrochemical *in situ* CSERS spectra of (a) Au@Co and (b) Au@PtCo in 0.1 M KOH solution. DFT calculated models of (c) O_2^- adsorbed on Pt (111) surface with a top site, (d) OH* adsorbed on PtCo (111) surface with a Co top site, and (e) O_2^- adsorbed on PtCo (111) surface with a Pt top site. Ru, Pt, O, and H atoms are showed as blue, silver, red, and white balls, respectively.

and the band at 1152 cm^{-1} does not shift, indicating that the bands at 853 and 1152 cm^{-1} are assigned to OH* and O_2^- species, respectively. DFT calculations also show the close frequencies about OH* and O_2^- species on PtCo surface and reveal that the adsorbed site of OH* is Co top site and O_2^- is Pt top site shown in Figs. 4(d) and 4(e) (the frequencies in Table S2 in the ESM). There is a collection of interfacial species on Co and Pt surfaces. We note that the band at 853 cm^{-1} of OH* is quite weaker than on pure Co surface. This is due to the low content of Co in the PtCo alloy shell (the content results in Table S1 in the ESM). There is a slight decrease in frequency of OH* and a slight increase in frequency of O_2^- on PtCo than on Pt surface.

3 Conclusions

In summary, electrochemical CSERS was used to systematically investigate the composition and evolution processes of interfacial species adsorbed on Pt, Co, and PtCo alloy surfaces and obtain direct spectral evidences of OH*, O_2^-, and metal oxide. There is obvious adsorption of oxygen species on Pt, Co, and PtCo alloy surfaces. During the *in situ* electrochemical Raman process, the adsorbed OH* and α-$Co(OH)_2$ exist on the Au@Co surface at lower potentials, and the OH* will disappear and the Co shell becomes high valence oxide at higher potentials. Meanwhile, on Au@Pt surface, only O_2^- species is observed on Pt surface during *in situ* experiment. The accumulation of OH* and O_2^- on the surface of PtCo alloy is observed. With this information and experimental capability, our results help understand more deeply about the interfacial electrocatalytic reaction process and mechanism.

Acknowledgements

This work was financially supported by the National Key Research and Development Program of China (No. 2020YFB1505800), the National Natural Science Foundation of China (Nos. 21925404 and 22021001), the Shenzhen Science and Technology Research Grant (No. JCYJ20200109140416788), the Science and Technology Program of Fujian Province (No. 2021Y01010295), the Youth Talent Support Program of Fujian Province (Eyas Plan of Fujian Province 2021), Research Initiation Fund of Jimei University (No. ZQ2021008), the Natural Science Foundation of Fujian Province of China (No. 2021J06001), and the China Postdoctoral Science Foundation (Nos. 2021TQ0188 and 2021M691874).

Electronic Supplementary Material: Supplementary material (the preparation procedures of nanoparticles, electrochemical setup, *in situ* Raman experiment, and DFT simulation) is available in the online version of this article at https://doi.org/10.1007/s12274-023-5473-9.

References

[1] Subbaraman, R.; Tripkovic, D.; Strmcnik, D.; Chang, K. C.; Uchimura, M.; Paulikas, A. P.; Stamenkovic, V.; Markovic, N. M. Enhancing hydrogen evolution activity in water splitting by tailoring Li^+-$Ni(OH)_2$-Pt interfaces. *Science* **2011**, *334*, 1256–1260.

[2] Wang, Y. H.; Zheng, S. S.; Yang, W. M.; Zhou, R. Y.; He, Q. F.; Radjenovic, P.; Dong, J. C.; Li, S. N.; Zheng, J. X.; Yang, Z. L. et al. *In situ* Raman spectroscopy reveals the structure and dissociation of interfacial water. *Nature* **2021**, *600*, 81–85.

[3] Ramaswamy, N.; Mukerjee, S. Alkaline anion-exchange membrane fuel cells: Challenges in electrocatalysis and interfacial charge transfer. *Chem. Rev.* **2019**, *119*, 11945–11979.

[4] Wang, T.; Zhang, Y. R.; Huang, B. T.; Cai, B.; Rao, R. R.; Giordano, L.; Sun, S. G.; Shao-Horn, Y. Enhancing oxygen reduction electrocatalysis by tuning interfacial hydrogen bonds. *Nat. Catal.* **2021**, *4*, 753–762.

[5] Tian, X. L.; Zhao, X.; Su, Y. Q.; Wang, L. J.; Wang, H. M.; Dang, D.; Chi, B.; Liu, H. F.; Hensen, E. J. M.; Lou, X. W. et al. Engineering bunched Pt-Ni alloy nanocages for efficient oxygen reduction in practical fuel cells. *Science* **2019**, *366*, 850–856.

[6] Li, P.; Jiang, Y. L.; Hu, Y. C.; Men, Y.; Liu, Y. W.; Cai, W. B.; Chen, S. L. Hydrogen bond network connectivity in the electric double layer dominates the kinetic pH effect in hydrogen electrocatalysis on Pt. *Nat. Catal.* **2022**, *5*, 900–911.

[7] Zhu, S. Q.; Qin, X. P.; Xiao, F.; Yang, S. L.; Xu, Y.; Tan, Z.; Li, J. D.; Yan, J. W.; Chen, Q.; Chen, M. S. et al. The role of ruthenium in improving the kinetics of hydrogen oxidation and evolution reactions of platinum. *Nat. Catal.* **2021**, *4*, 711–718.

[8] Li, H. Q.; Zeng, R.; Feng, X. R.; Wang, H. S.; Xu, W. X.; Lu, X. Y.; Xie, Z. X.; Abruña, H. D. Oxidative stability matters: A case study of palladium hydride nanosheets for alkaline fuel cells. *J. Am. Chem. Soc.* **2022**, *144*, 8106–8114.

[9] Wei, J.; Zheng, Y. L.; Li, Z. Y.; Xu, M. L.; Chen, Y. X.; Ye, S. Electrochemistry of oxygen at Ir single crystalline electrodes in acid. *Electrochim. Acta* **2017**, *246*, 329–337.

[10] Chen, F. Y.; Wu, Z. Y.; Gupta, S.; Rivera, D. J.; Lambeets, S. V.; Pecaut, S.; Kim, J. Y. T.; Zhu, P.; Finfrock, Y. Z.; Meira, D. M. et al. Efficient conversion of low-concentration nitrate sources into ammonia on a Ru-dispersed Cu nanowire electrocatalyst. *Nat. Nanotechnol.* **2022**, *17*, 759–767.

[11] Zhu, J.; Hu, L. S.; Zhao, P. X.; Lee, L. Y. S.; Wong, K. Y. Recent advances in electrocatalytic hydrogen evolution using nanoparticles. *Chem. Rev.* **2020**, *120*, 851–918.

[12] Wang, L.; Zeng, Z. H.; Gao, W. P.; Maxson, T.; Raciti, D.; Giroux, M.; Pan, X. Q.; Wang, C.; Greeley, J. Tunable intrinsic strain in two-dimensional transition metal electrocatalysts. *Science* **2019**, *363*, 870–874.

[13] Seh, Z. W.; Kibsgaard, J.; Dickens, C. F.; Chorkendorff, I.; Nørskov, J. K.; Jaramillo, T. F. Combining theory and experiment in electrocatalysis: Insights into materials design. *Science* **2017**, *355*, eaad4998.

[14] Ledezma-Yanez, I.; Wallace, W. D. Z.; Sebastián-Pascual, P.; Climent, V.; Feliu, J. M.; Koper, M. T. M. Interfacial water reorganization as a pH-dependent descriptor of the hydrogen evolution rate on platinum electrodes. *Nat. Energy* **2017**, *2*, 17031.

[15] Strmcnik, D.; Uchimura, M.; Wang, C.; Subbaraman, R.; Danilovic, N.; van der Vliet, D.; Paulikas, A. P.; Stamenkovic, V. R.; Markovic, N. M. Improving the hydrogen oxidation reaction rate by promotion of hydroxyl adsorption. *Nat. Chem.* **2013**, *5*, 300–306.

[16] Subbaraman, R.; Tripkovic, D.; Chang, K. C.; Strmcnik, D.; Paulikas, A. P.; Hirunsit, P.; Chan, M.; Greeley, J.; Stamenkovic, V.; Markovic, N. M. Trends in activity for the water electrolyser reactions on 3d M (Ni, Co, Fe, Mn) hydr(oxy)oxide catalysts. *Nat. Mater.* **2012**, *11*, 550–557.

[17] Lu, S. Q.; Zhuang, Z. B. Investigating the influences of the adsorbed species on catalytic activity for hydrogen oxidation reaction in alkaline electrolyte. *J. Am. Chem. Soc.* **2017**, *139*, 5156–5163.

[18] Li, J. F.; Huang, Y. F.; Ding, Y.; Yang, Z. L.; Li, S. B.; Zhou, X. S.; Fan, F. R.; Zhang, W.; Zhou, Z. Y.; Wu, D. Y. et al. Shell-isolated nanoparticle-enhanced Raman spectroscopy. *Nature* **2010**, *464*, 392–395.

[19] Davis, J. G.; Gierszal, K. P.; Wang, P.; Ben-Amotz, D. Water structural transformation at molecular hydrophobic interfaces. *Nature* **2012**, *491*, 582–585.

[20] Li, J. F.; Zhang, Y. J.; Ding, S. Y.; Panneerselvam, R.; Tian, Z. Q. Core–shell nanoparticle-enhanced Raman spectroscopy. *Chem. Rev.* **2017**, *117*, 5002–5069.

[21] Nie, S. M.; Emory, S. R. Probing single molecules and single nanoparticles by surface-enhanced Raman scattering. *Science* **1997**, *275*, 1102–1106.

[22] Wang, Y. H.; Wei, J.; Radjenovic, P.; Tian, Z. Q.; Li, J. F. *In situ* analysis of surface catalytic reactions using shell-isolated nanoparticle-enhanced Raman spectroscopy. *Anal. Chem.* **2019**, *91*, 1675–1685.

[23] Zou, Y. X.; Chen, L.; Song, Z. L.; Ding, D.; Chen, Y. Q.; Xu, Y. T.; Wang, S. S.; Lai, X. F.; Zhang, Y.; Sun, Y. et al. Stable and unique graphitic Raman internal standard nanocapsules for surface-enhanced Raman spectroscopy quantitative analysis. *Nano Res.* **2016**, *9*, 1418–1425.

[24] Huang, Y. F.; Kooyman, P. J.; Koper, M. T. M. Intermediate stages of electrochemical oxidation of single-crystalline platinum revealed by *in situ* Raman spectroscopy. *Nat. Commun.* **2016**, *7*, 12440.

[25] Jing, C.; Yuan, T. T.; Li, L. L.; Li, J. F.; Qian, Z. X.; Zhou, J.; Wang, Y. F.; Xi, S. B.; Zhang, N.; Lin, H. J. et al. Electrocatalyst with dynamic formation of the dual-active site from the dual pathway observed by *in situ* Raman spectroscopy. *ACS Catal.* **2022**, *12*, 10276–10284.

[26] Das, A.; Mohapatra, B.; Kamboj, V.; Ranjan, C. Promotion of electrochemical water oxidation activity of Au supported cobalt oxide upon addition of Cr: Insights using *in situ* Raman spectroscopy. *ChemCatChem* **2021**, *13*, 2053–2063.

[27] Fester, J.; Makoveev, A.; Grumelli, D.; Gutzler, R.; Sun, Z. Z.; Rodríguez-Fernández, J.; Kern, K.; Lauritsen, J. V. The structure of the cobalt oxide/Au catalyst interface in electrochemical water splitting. *Angew. Chem., Int. Ed.* **2018**, *57*, 11893–11897.

[28] Antolini, E.; Salgado, J. R. C.; Gonzalez, E. R. The stability of Pt-M (M = first row transition metal) alloy catalysts and its effect on the activity in low temperature fuel cells: A literature review and tests on a Pt-Co catalyst. *J. Power Sources* **2006**, *160*, 957–968.

[29] Dong, J. C.; Zhang, X. G.; Briega-Martos, V.; Jin, X.; Yang, J.; Chen, S.; Yang, Z. L.; Wu, D. Y.; Feliu, J. M.; Williams, C. T. et al. *In situ* Raman spectroscopic evidence for oxygen reduction reaction intermediates at platinum single-crystal surfaces. *Nat. Energy* **2019**, *4*, 60–67.